Monthly Notices
of the
ROYAL ASTRONOMICAL SOCIETY

MNRAS **451,** 3898–3908 (2015) doi:10.1093/mnras/stv1229

Luminosity–time and luminosity–luminosity correlations for GRB prompt and afterglow plateau emissions

M. Dainotti,[1,2⋆] V. Petrosian,[1] R. Willingale,[3] P. O'Brien,[3] M. Ostrowski[2] and S. Nagataki[4]

[1]*Astronomy Department, Stanford University, Via Pueblo Mall 382, Stanford, CA, USA*
[2]*Obserwatorium Astronomiczne, Uniwersytet Jagielloński, ul. Orla 171, PL-30-244 Kraków, Poland*
[3]*Department of Physics and Astronomy, University of Leicester, Road Leicester LE1 7RH, UK*
[4]*Astrophysical Big Bang Laboratory, Riken, Wako, Saitama 351-0198, Japan*

Accepted 2015 May 28. Received 2015 May 4; in original form 2014 July 31

ABSTRACT

We present an analysis of 123 gamma-ray bursts (GRBs) with known redshifts possessing an afterglow plateau phase. We reveal that L_a-T_a^* correlation between the X-ray luminosity L_a at the end of the plateau phase and the plateau duration, T_a^*, in the GRB rest frame has a power-law slope different, within more than 2σ, from the slope of the prompt L_f-T_f^* correlation between the isotropic pulse peak luminosity, L_f, and the pulse duration, T_f^*, from the time since the GRB ejection. Analogously, we show differences between the prompt and plateau phases in the energy duration distributions with the afterglow emitted energy being on average 10 per cent of the prompt emission. Moreover, the distribution of prompt pulse versus afterglow spectral indexes does not show any correlation. In the further analysis we demonstrate that the L_{peak}–L_a distribution, where L_{peak} is the peak luminosity from the start of the burst, is characterized with a considerably higher Spearman correlation coefficient, $\rho = 0.79$, than the one involving the averaged prompt luminosity, L_{prompt}–L_a, for the same GRB sample, yielding $\rho = 0.60$. Since some of this correlation could result from the redshift dependences of the luminosities, namely from their cosmological evolution we use the Efron–Petrosian method to reveal the intrinsic nature of this correlation. We find that a substantial part of the correlation is intrinsic. We apply a partial correlation coefficient to the new de-evolved luminosities showing that the intrinsic correlation exists.

Key words: methods: data analysis – methods: statistical – gamma-ray burst: general – cosmological parameters.

1 INTRODUCTION

Gamma-ray bursts (GRBs) are the most distant and most luminous object observed in the Universe with redshifts up to $z \approx 9.4$ and isotropic energies up to 10^{54} erg. Discovering universal properties is crucial in understanding the processes responsible for the GRB phenomenon. However, GRBs seem to be anything but standard candles, with their energetics spanning over eight orders of magnitude. There have been numerous attempts to standardize GRB by finding some correlations among the observables, which can then be used for cosmological studies. Examples of these are the claimed correlations between the isotropic total prompt emitted energy E_{iso} and the peak photon energy of the νF_ν spectrum E_{peak} (Lloyd & Petrosian 1999; Amati et al. 2002; Amati, Frontera & Guidorzi 2009), the beaming corrected energy E_γ and E_{peak} (Ghirlanda, Ghisellini & Lazzati 2004; Ghirlanda, Ghisellini & Firmani 2006), the luminosity L and E_{peak} (Schaefer 2003; Yonekotu et al. 2004) and luminosity and variability V (Fenimore & Ramirez-Ruiz 2000; Riechart et al. 2001). However, because of the large dispersion in these relations (Butler et al. 2007; Butler, Kocevski & Bloom 2009; Yu, Qi & Lu 2009) and possible impact of detector thresholds, the utility of these correlation as a proxy for standard candle and cosmological studies (Shahmoradi & Nemiroff 2009) have been questioned (Cabrera et al. 2007; Collazzi & Schaefer 2008).

In this paper we investigate whether some common features may be identified in the light curves during both the prompt and afterglow phases. A crucial breakthrough in this field has been the observation of GRBs by the *Swift* satellite, launched in 2004. The onboard instruments Burst Alert Telescope (BAT; 15–150 keV), X-Ray Telescope (XRT; 0.3–10 keV) and Ultraviolet/Optical Telescope (UVOT; 170–650 nm) provide a broad wavelength coverage

⋆ E-mail: mariagiovannadainotti@yahoo.it

and a rapid follow-up of the afterglows. *Swift* has revealed a complex behaviour of the light curves (O'Brien et al. 2006; Sakamoto et al. 2007), where one can distinguish two, three or even more segments in the afterglow. The second segment, when it is flat, is called the plateau emission. Investigating the X-ray afterglow, Dainotti, Cardone & Capozziello (2008) and Dainotti et al. (2010) discovered a power-law (PL) anticorrelation between the rest-frame time T_a^*, when the plateau ends and a PL decay phase begins, and L_a, the isotropic X-ray luminosity at T_a^*.[1] This correlation has also been reproduced independently by other authors with slopes within 1σ of the above value (Ghisellini et al. 2009; Sultana, Kazanas & Fukumura 2012).[2] However, some of this correlation is induced by the redshift dependences of the variables. More recently, Dainotti et al. (2013a) have demonstrated that after correcting for this observational bias there remains a significant (at 12σ level) anticorrelation with the intrinsic slope $b = -1.07^{+009}_{-0.14}$.

The L_a-T_a^* anticorrelation has been a useful test for theoretical interpretation of GRB models involving accretion (Cannizzo & Gehrels 2009; Cannizzo, Troja & Gehrels 2011), a magnetar (Dall'Osso et al. 2011; O'Brien, Lyons & Rowlinson 2011; Rowlinson et al. 2013, 2014; Bernardini et al. 2012a,b), the long-lived reverse shock models (Leventis, Wijers & van der Horst 2014; Van Erten 2014b) and other additional models such as the prior emission model (Yamazaki 2009), the unified GRB and active galactic nucleus (AGN) model (Nemmen et al. 2012) and the induced gravitational collapse scenario (Izzo et al. 2012). There are several models, e.g. the photospheric emission model (Ito et al. 2014), that can account for this observed correlation. In addition, Dainotti et al. (2011a) attempted to use this relation as a redshift estimator and Cardone, Capozziello & Dainotti (2009), Cardone et al. (2010) and Postnikov et al. (2014) have used it for cosmological studies. But Dainotti et al. (2013b) have described some caveats on the use of non-intrinsic correlations to constrain cosmological parameters. Dainotti et al. (2015) used this correlation to evaluate the redshift-dependent ratio $\Psi(z) = (1+z)^{\alpha}$ of the GRB rate to the star formation rate.

The aim of this paper is to compare similar luminosity–duration correlations in the light curve of the prompt emission with the afterglow ones. This may shed light on the relative energizing, dissipation and radiative processes of afterglow and prompt emission. Dainotti et al. (2011b) have demonstrated the existence of a tight correlation between the afterglow luminosity L_a and the average L_{prompt} luminosity over all the prompt emission phase. Moreover, Qi & Lu (2010) have discovered for the first time the existence of luminosity–duration anticorrelation in the prompt emission. Later, Sultana et al. (2012) used a sample of 12 GRBs to show that the burst peak isotropic luminosity, L_{peak}, and the spectral lag, τ, distribution continuously extrapolates into the L_a-T_a^* distribution, with a common correlation slope close to -1.0. The authors conclude that, if indeed the underlying physics is common, it should be of kinematic origin. Because the lag time τ is somewhat different variable than the durations in the light curves, we propose a more direct comparison between the L_a-T_a^* correlation and the L_f–T_f^*, where L_f and T_f^* stand for the peak luminosity and pulse width of individual gamma-ray pulses in the prompt emission. We here use the same notation of L_f and T_f following the original notation of Willingale et al. (2010, hereafter W10). Because the W07 model masks out the flares in the light curve, we use the W10 model which is more appropriate for dealing with individual pulses. In the next section we present the theoretical motivations for this data analysis and what can be learned from the results. In Section 3 we describe the modelling of the light curves, and in Section 4 we describe the data analysis. The results on the luminosity–duration correlation are presented in Section 5, and a brief summary and discussion is presented in Section 6.

[1] Here, and subsequently, * denotes the rest-frame quantities. These quantities are obtained by fitting the light curves to the phenomenological Willingale et al. (2007, hereafter W07) model and all luminosities and the respective derived energies are for an assumed isotropic emission. To simplify the notation we omit the subscript 'iso'.

[2] A luminosity–time (L–T) correlation has been found also for short GRBs with extended emission (Dainotti et al. 2010) and future perspective will be the investigation of this class of GRBs within the model of Barkov & Pozanenko (2011).

2 THEORETICAL MOTIVATION

To start we summarize some selected models in the literature which address the luminosity–duration correlations and attempt to explain the observed luminosity prompt–afterglow correlations.

(1) The commonly invoked cause of the plateau formation by continuous energy injection into the GRB generated forward shock leads to an efficiency crisis for the prompt mechanism as soon as the plateau duration exceeds 10^3 s. Hascoet et al. (2014) studied two possible alternatives: the first one within the framework of the standard forward shock model but allows for a variation of the microphysics parameters to reduce the radiative efficiency at early times; in the second scenario the early afterglow results from a long-lived reverse shock in the forward shock scenario. In both scenarios the plateaus following the prompt–afterglow correlations can be obtained under the condition that additional parameters are added. In the forward shock scenario the preferred model supposes a wind external medium and a microphysics parameter ϵ_e, the fraction of the internal energy that goes into electrons (or positrons) and can in principle be radiated away. This varies as n^{ν} (where n is the external density), with $\nu \approx 1$ to obtain a flat plateau. They conclude that acting on one single parameter can lead to the formation of a plateau that also satisfies the observed prompt–afterglow correlations presented in Dainotti et al. (2011b). Another possibility presented by Hascoet et al. (2014) is the reverse shock scenario, in which the typical Lorentz factor of the ejecta should increase with burst energy to satisfy the prompt–afterglow relations, more in particular the ejecta must contain a tail of low Lorentz factor with a peak of energy deposition at $\Gamma \geq 10$.

(2) Van Erten (2014a) shows that the observed L_{prompt}–$L_{afterglow}$ correlations rule out basic thin shell models but not basic thick ones. In the thick shell case, both forward shock and reverse shock outflows are shown to be consistent with the correlations, through randomly generated samples of thick shell model afterglows. A more strict approach with the standard assumption on relativistic blast waves is used in the contexts of both thick and thin shell models. In the thin shell model, the afterglow plateau phase is the result of the pre-deceleration emission from a slower component in a two-component or jet-type model. For thick shells, the plateau phase results from energy injection either in the form of late central source activity or via additional kinetic energy transfer from slower ejecta which catches up with the blast wave. It is shown that thin shell models cannot be reconciled with the observed L–T correlation and, then, it is inferred the existence of a correlation between the plateau end time and the ejecta energy that is not seen in the observational data. However, this does not mean that acceptable fits using a thin shell model are not possible, it might even be possible

to successfully fit all the bursts with plateau stages. Thick shell models, on the other hand, can easily reproduce the *L*–*T* correlation even if uncorrelated values for the model parameters are applied in modelling. In this context it is difficult to distinguish between forward shock and reverse shock emission dominated models, or homogeneous and stellar wind-type environments.

(3) A supercritical pile-up model (Sultana, Kazanas & Mastichiadis 2013) provides an explanation for both the steep-decline-and-plateau or the steep-decline-and-PL-decay structures of the GRB afterglow phase, as observed in a large number of light curves, and to the *L*–*T* relation. Since in this model, the detailed calculations of an estimate of the energy of the prompt is needed, it would be relevant to evaluate if the $L_{\rm prompt}$–$L_{\rm afterglow}$ and the $L_{\rm peak}$–$T_{\rm peak}$ relations, as defined here, can be reproduced.

(4) Ruffini et al. (2014) show that the induced gravitational collapse paradigm is able to reproduce the $L_{\rm a}$–$L_{\rm prompt}$ relations very tightly. More in general, this model addresses the very energetic (10^{52}–10^{54} erg) long GRBs associated with supernovae. They manage to reproduce the light curves giving different scenarios for the circumburst medium, with either a radial structure for the wind (Guida et al. 2008) or with a fragmentation of the shell (Dainotti et al. 2007) thus well fitting the afterglow plateau and the prompt emission.

Given this wide possible theoretical interpretations it is important to take into consideration additional information from the observational correlations presented in this paper. This can help to provide new constraints for the physical models of GRB explosion mechanism.

3 MODELLING THE GRB LIGHT CURVES

Usually the X-ray light curves of afterglows observed by XRT are modelled using a series of PLs segments plus pulses (see e.g. Evans et al. 2009, 2010, 2014; Margutti et al. 2013). Here we use a different approach whereby we fit the light curves to the analytic functional forms of W10, which, as mentioned above, is an improved version of W07 and fits the complete BAT+XRT light curves without masking the X-ray flares. This procedure uses somewhat physically motivated pulse profile for the prompt emission, based on the spherical expanding shell model (Ryde & Petrosian 2002; Dermer 2007), where the shells are energized during the rise of the pulse and the decay phase of the pulse involves emission generated further away from the line of sight that arrive latter and with a smaller Doppler boost.

The peak luminosity and pulse width of the individual pulse are denoted as $L_{\rm f}$ and $T_{\rm f}$ while $L_{\rm a}$ and $T_{\rm a}$ refer to the afterglow values define above. Fig. 1 shows these quantities for a schematic light curve. We also determine the total energy fluence E for pulses and the afterglow phase. The rest-frame times $T_{\rm f}^*$ and $T_{\rm a}^*$ represent the times when the respective energy supply is switched off.

3.1 Nomenclature

For clarity we report a summary of the nomenclature adopted in the paper (cf. Fig. 1). All times described below are given in the observer frame, while with the upper index * we denote in the text the observables in the GRB rest frame. All considered energies and luminosities are derived assuming the isotropic emission.

(i) $T_{\rm peak}$, is the peak luminosity time in the prompt emission, measured since the start of the burst. Its corresponding luminosity is $L_{\rm peak}$.

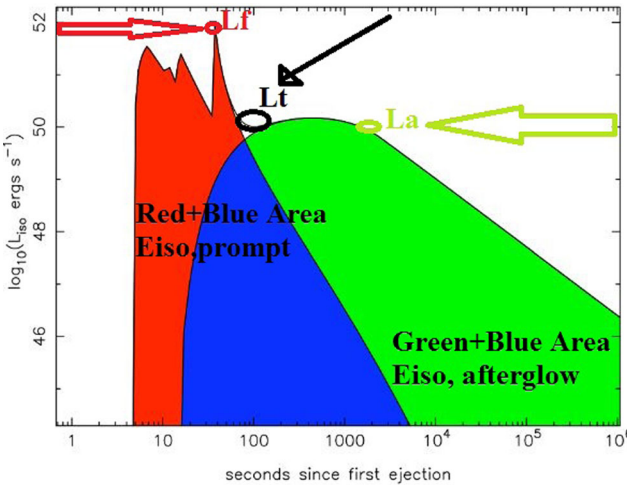

Figure 1. A schematic light curve which illustrates how the prompt and afterglow emission components are integrated to obtain the respective energies within the W010 model. The red+blue area is proportional to the energy of the prompt emission, where we also indicated the time $T_{\rm f}$, the duration of the pulse since the time of the GRB ejection. The green one+the blue area indicates the afterglow's energy, where $T_{\rm a}$ is the time of the end of the plateau emission. In the joint area (blue) $T_{\rm t}$ is the time where the luminosities of the decaying prompt emission and the afterglow emission are equal. The solid line is the total luminosity.

(ii) $T_{\rm f}$ is the pulse peak time in the prompt emission computed from the GRB ejection time, $T_{\rm ej}$. Its corresponding luminosity is $L_{\rm f}$.

(iii) $T_{\rm prompt}$ is the sum of all the pulse peak times, $T_{\rm f}$, for each GRB in the prompt.

(iv) T_{90} is the time between the 5 and 95 per cent of the energy released in the GRB prompt phase.

(v) T_{45} is the time between the 5 and 50 per cent of the energy released in the GRB prompt phase.

(vi) L and T indicate the luminosity and time which can be either for the prompt ($L_{\rm f}$ or $L_{\rm peak}$; $T_{\rm f}$ or $T_{\rm peak}$) or the afterglow ($L_{\rm a}$; $T_{\rm a}$) emission. The equivalent energy–duration E and T relations are also considered.

(vii) $E_{\rm min}$ and $E_{\rm max}$ are, respectively, the minimum and maximum energy in the bandpass of the instrument. For the XRT a respective range is (0.3, 10) keV, while for the BAT it is (15, 150) keV.

4 DATA ANALYSIS

We have analysed the sample of long GRBs with known redshifts detected by *Swift* from 2005 January up to 2011 September, for which the light curves include early XRT data. The redshifts z are taken from J. Greiner's web site[3] and from Xiao & Schaefer (2009). Among these GRBs we have selected 123 with early XRT coverage for the fitting. Thus, the BAT–XRT combined data give us almost continuous monitoring of the GRB varying emission. On the other hand, we rejected all bursts where a gap in the XRT coverage reveal flares with only partial coverage, missing the turn on, the peak and/or the decay phases. For both prompt and afterglow components we compute the luminosity in the appropriate energy bandpass, ($E_{\rm min}$, $E_{\rm max}$), as

$$L(E_{\rm min}, E_{\rm max}, t) = 4\pi D_L^2(z)\, F(t) K(E_{\rm min}, E_{\rm max}), \quad (1)$$

[3] http://www.mpe.mpg.de/~jcg/grbgen.html

where $D_L(z)$ is the luminosity distance computed in the flat Λ cold dark matter (ΛCDM) cosmological model with $\Omega_M = 0.291$ and $h = 0.70$ in units of 100 km s^{-1} Mpc^{-1}, F is the measured X-ray energy flux and K is the K-correction for the cosmic expansion (Bloom, Frail & Sari 2001):

$$K = \frac{\int_{E_{\rm min}/(1+z)}^{E_{\rm max}/(1+z)} \Phi(E){\rm d}E}{\int_{E_{\rm min}}^{E_{\rm max}} \Phi(E){\rm d}E}, \quad (2)$$

where the energy spectrum $\Phi(E)$ of the afterglows is described by a simple PL $\Phi(E) = E^{-\beta_{\rm a}}$, while the one of the prompt pulses by the Band function (Band et al. 1993).[4]

We also employ another way to compute $L_{\rm peak}$, instead of using the functional form of W10, we follow Schaefer (2007) and equation (1), using the brightest peak flux over 1 s interval.[5] For the functional form for the spectrum, we use either a PL or a PL with a cut-off (CPL), depending on the best χ^2 fit presented in the second BAT catalogue (differently from the approach used in W010 in which the Band function for the pulse profile is adopted). All of the BAT spectra are acceptably fitted by either a PL or a CPL model. The same criterion as in the first BAT catalogue, $\Delta\chi^2$ between a PL and a CPL fit greater than 6 ($\Delta\chi^2 \equiv \Delta\chi^2_{\rm PL} - \Delta\chi^2_{\rm CPL}$), was used to determine if the CPL model is a better spectral model for the data. Note that none of the BAT spectra shows a significant improvement in $\Delta\chi^2$ with a Band function (Band et al. 1993) fit compared to that of a CPL model fit. For GRBs not presented in the catalogue we have chosen the spectral energy distribution as a function that gives the best χ^2 according to the *Swift* Burst Analyser, http://www.swift.ac.uk/burstanalyser/ (Evans et al. 2009), which is consistent with the approach of the second BAT catalogue. For the derivation of the pulse energy we integrated the fitted model luminosity curve for each pulse as follows:

$$E_{\rm pulse} = \int_{T_0}^{T_{\rm end}} 4\pi D_L^2(z)\, F(t)\, K(E_{\rm min}, E_{\rm max}){\rm d}t, \quad (3)$$

where $T_0 = T_{\rm f} - T_{\rm ej}$ following the W010 notation, while $T_{\rm end}$ is the time end of the pulse width, for these definitions see Section 3.1. The energy is presented on the lower panel of Fig. 2.

In what follows we use the above data for comparing the prompt and afterglow characteristics and correlations.

5 RESULTS

The results are presented in Fig. 2. The top panel shows the L–T scatter diagram including both pulses ($L_{\rm f}$-$T_{\rm f}^*$, black points) and the afterglow ($L_{\rm a}$-$T_{\rm a}^*$, red points) while the middle panel shows the energy, E–T, scatter diagram, where the afterglow energy is calculate as $E_{\rm a} = L_{\rm a}T_{\rm a}^*$. The lower panel shows the distribution on number of pulses per GRB. For each GRB we also show the brightest luminosity (integrated over 1 s) $L_{\rm f,\,max}$ (green) and $E_{\rm peak,\,max}$ (yellow) taken as the maximum $L_{\rm f}$ and $E_{\rm peak}$ among the pulses of a given GRB.[6] We first note that using the new and larger sample we have repeated the analysis carried out in Dainotti et al. (2013a) on the $L_{\rm a}$-$T_{\rm a}^*$ correlation and find similar results. A fit to this relation $\log L_{\rm a} = \log a + b \log T_{\rm a}^*$ using a Bayesian method (D'Agostini 2005) yields the observed intercept $\log a_{\rm plateau} = 51.14 \pm 0.58$ and

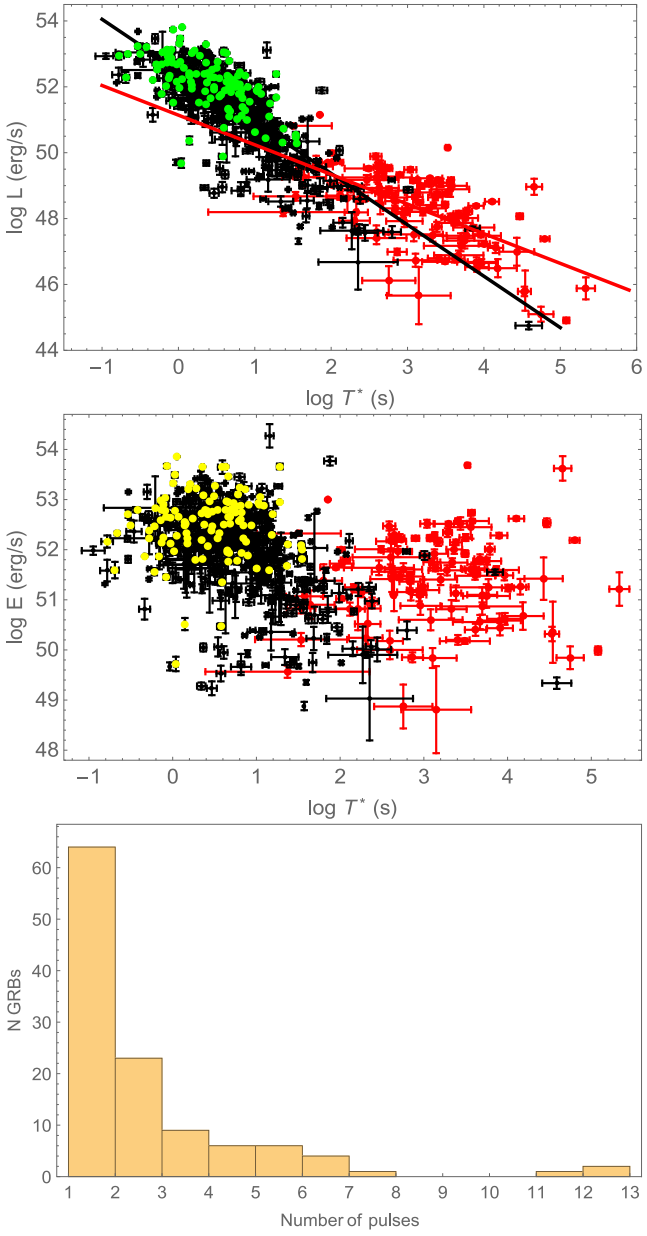

Figure 2. Distributions of L versus T^* (upper panel) and E versus T^* (middle panel) for each single pulse both in the prompt (black symbols) and in the afterglow (red symbols) emissions. L and E are equal to $L_{\rm f}$ and $E_{\rm f}$ for the prompt emission pulses, while being equal to $L_{\rm a}$ and $E_{\rm afterglow} = L_{\rm a}T_{\rm a}^*$ for the afterglows, and, respectively, the time T^* represents $T_{\rm f}^*$ for the prompt emission pulses and $T_{\rm a}^*$ for the afterglow phase. The green points represent the highest luminosity prompt emission pulses ($T_{L_{\rm max}}, L_{\rm max}$), while the yellow ones represent ($T_{E_{\rm max}}$, $E_{\rm max}$). In the bottom panel, we show a distribution of the number of maximum luminosity pulses in the GRB pulse histogram.

[4] For the prompt pulses $\beta_{\rm pulse}$ is the low-energy index of the Band spectrum and the spectral fits are calculated separately from the afterglow ones within the ($E_{\rm min}$, $E_{\rm max}$) = (15–150) keV in the four BAT energy channels (15–25, 25–50, 50–100 and 100–150 keV). We point out here that the spectrum is not extrapolated at low energy in the afterglow, but it has been computed separately. Moreover, in the afterglow phase generally there is no spectral evolution; few bursts which show spectral evolution are not in our list of GRBs.

[5] In our sample there is always a peak flux defined for 1 s interval.

[6] We note that the catalogue uses a PL or a PL with an exponential break, instead of the Band function, for the spectral fitting.

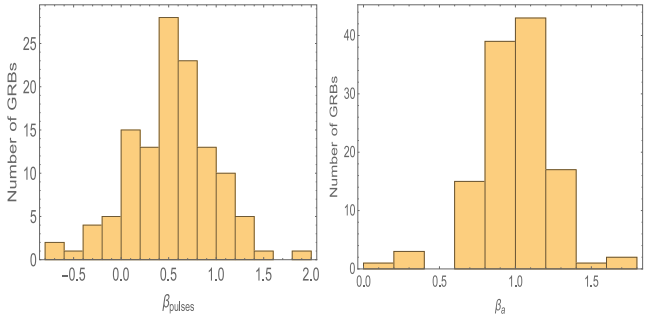

Figure 3. Spectral index distributions for the prompt emission pulses, $\beta_{\rm pulses}$ (left-hand panel); the pulses in the afterglow phase (right-hand panel), $\beta_{\rm a}$. We represent all the pulses both in the prompt and in the afterglow emission.

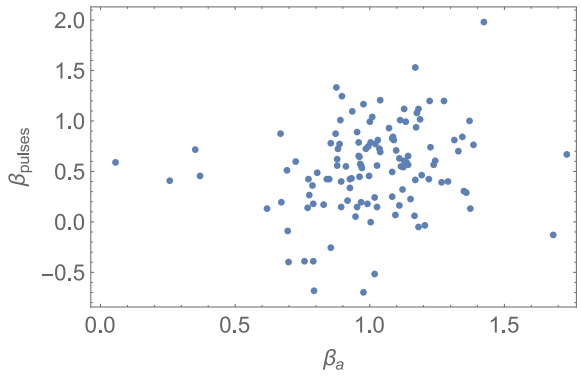

Figure 4. Spectral index distribution of the averaged $\beta_{\rm pulses}$ among the pulses in each GRB versus $\beta_{\rm a}$ both computed within the W010 model. We note that there is no correlation among the two distributions.

slope $b_{\rm plateau} = -0.90^{+0.19}_{-0.17}$ and the probability of the correlation occurring by chance for an uncorrelated sample is $P \approx 10^{-35}$ (Bevington & Robinson 2003).

5.1 The *L*-*T* correlations

As shown in the upper panel of Fig. 2 there is a strong L–T^* anticorrelation for both the prompt pulses and the plateau. Linear fits to $\log L$ versus $\log T$ using the D'Agostini method (D'Agostini 2005) described in Appendix APPENDIX A:, yield slopes and intercepts, respectively, to be $b_{\rm prompt} = -1.52^{+0.13}_{-0.11}$, $\log a_{\rm prompt} = 52.98 \pm 0.08$ erg s^{-1} for the prompt pulses, and $b_{\rm plateau} = -0.90^{+0.19}_{-0.17}$, $\log a_{\rm plateau} = 51.14 \pm 0.58$ for the plateau. The slopes differ almost by 3σ implying a significance difference at least in the observed correlations. More credence can be given to this result, because we have used the same W10 method for determining the luminosities and duration for both prompt and afterglow components. This makes the comparison between $L_{\rm f}$–$T^*_{\rm f}$ and $L_{\rm a}$-$T^*_{\rm a}$ well defined. It has already been demonstrated within the context of W07 that both prompt and afterglow emission can be represented by the same functional form. The underlying hypothesis, which we test here, is that the plateau can be considered as a single flare with origin similar to the peaks of the prompt emission. Another way to look at this correlation is to consider the energy–duration correlation, where the energy is computed integrating the pulse shape over the pulse width. As expected we see much shallower relation for energies than luminosities. The prompt pulses show still a weak anticorrelation, but there is no correlation between $E_{\rm a}$ and $T^*_{\rm a}$ for the plateau. The prompt emission pulses and the plateau data occupy two distinctive regions on the energy–duration plane. The pulses are short and have slightly higher average energy as compared to the plateau, which are in average 214 times longer. However, there is continuity in the distribution between prompt and plateau pulses, namely there is also a small region of overlapping among the two phases.

For clarity, in the lower panel of Fig. 2, we present the distribution of $L_{\rm max}$, which is the maximum value of $L_{\rm peak}$ in a burst, in correspondence of its peak number, namely at which the peak occurs. We note that the majority of $L_{\rm max}$ occur between the first and second peaks of the prompt emission, only in rare cases $L_{\rm max}$ corresponds to a peak number which exceeds 10.

5.2 Spectral features of the pulses

We now compare the spectral characteristics. Fig. 3 shows the distribution of spectral indexes of 628 prompt pulses and 123 from the afterglows. The two distributions are significantly different. The distribution of the prompt pulse indexes is broader than that of the afterglow. As mentioned above, the spectral index $\beta_{\rm a}$ does usually not evolve (Evans et al. 2014), it is constant over the plateau phase and later during the afterglow decay phase, while the values of $\beta_{\rm pulses}$ may vary during the prompt emission phase. In Fig. 4 we plot the average index of prompt pulses in each source versus the afterglow index. There seem to be very little correlation between the two indexes with most GRBs having a harder prompt than afterglow spectra.

Moreover, the spectral parameters do not correlate strongly with the other parameters we have introduced so far such as E, L and the various time-scales. When inspecting the Fig. 3, the spectral index of the pulses evolves and this evolution has been considered in the pulse model fit. Here, the spectrum of each single pulse has been computed. We note that the $\beta_{\rm pulses}$ computed for each pulse have wider distributions than the typical values, integrated over T_{90}, of β in the prompt phase. These differences in spectral index do not imply necessarily or justify a difference in the L–T correlation slopes. In fact, spectral breaks and spectral evolution can in principle explain their diverse distributions.

5.3 Luminosity–luminosity correlation

We now compare prompt energy–afterglow energy and prompt luminosity–afterglow luminosity correlations.

In Fig. 5 we compare the average prompt and the afterglow energies. The $\langle E_{\rm prompt}\rangle = \sum_{i=1}^{N} E_{{\rm pulse},i}/N$, where $E_{{\rm pulse},\,i}$ is the energy of each single pulse computed following equation (3) in each GRB and N is the number of pulses in each GRB. For the afterglow the average afterglow energy, $\langle E_{\rm afterglow}\rangle$, coincides with $E_{\rm afterglow}$ of the single pulses since we do not have multiple pulses in the afterglow in this sample, in fact $N = 1$ for each GRB afterglow. Previously W07 found that in few cases $E_{\rm afterglow} \equiv \langle E_{\rm prompt}\rangle$, but in most cases $E_{\rm afterglow}$ was roughly 10 per cent of the prompt emission. Here, with many more GRBs analysed and within the pulse-afterglow model we confirm this result.

The correlation of the prompt peak pulse isotropic luminosity averaged over all single GRB pulses and the afterglow luminosity computed within the W010 model is comparable with the one presented in the upper panel of Fig. 6, that correlates $L_{\rm peak}$, the isotropic peak luminosity of the brightest GRB prompt emission pulse from the time of the burst, and $L_{\rm a}$ where $L_{\rm peak}$ has been computed using the approach adopted in the second BAT catalogue (Sakamoto et al.

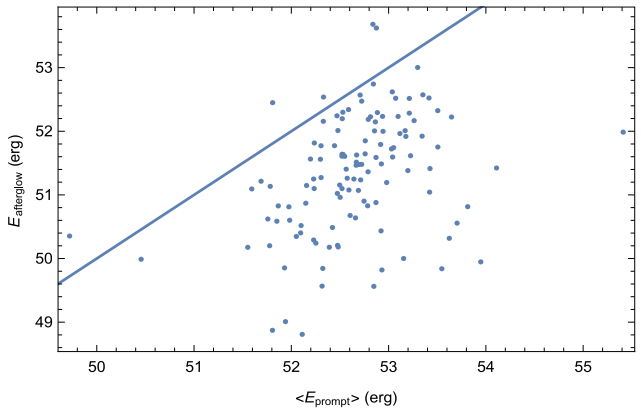

Figure 5. Prompt averaged energy $\langle E_{\rm prompt}\rangle$ versus afterglow energy, $E_{\rm afterglow}$, for 123 GRBs computed using the W010 model. The solid line for equal prompt and afterglow energies is provided for reference.

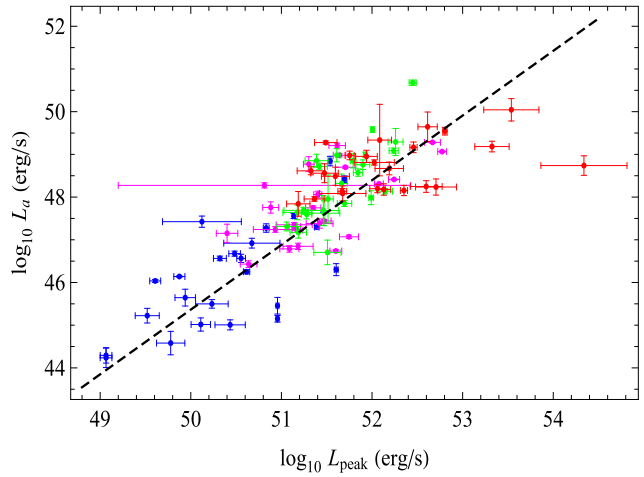

Figure 6. GRB distributions in redshift bins at $L_{\rm a}$–$L_{\rm peak}$ plane, where $L_{\rm peak}$ is computed using the approach used in the second BAT catalogue. The sample is splited into four different equipopulated redshift bins: $z \leq 0.84$ (blue), $0.84 \leq z < 1.8$ (magenta), $1.8 \leq z < 2.9$ (green) and $z \geq 2.9$ (red). The dashed line is the fitting correlation line.

2011), as described in Section 4. We have tested over all the GRB sample that $L_{\rm peak}$, presented in Fig. 6 (upper panel), has a consistent distribution compared to $L_{\rm f}$, obtained from the pulse fitting.

In Fig. 6 we show that the correlation between $L_{\rm peak}$ and $L_{\rm a}$ exists even for different redshift bins. The fitted correlation reads as follows:

$$\log L_{\rm a} = A + B\ \log L_{\rm peak}, \qquad (4)$$

where $A = -14.67 \pm 3.46$ and $B = 1.21^{+0.14}_{-0.13}$.

Dainotti et al. (2011b) demonstrated that correlations exist between $L_{\rm a}$ and the luminosities for the prompt emission, computed as E/T^*, where T^* are the characteristic GRB rest-frame time-scales $T^*_{\rm p} = T_{\rm p}/(1+z)$, $T^*_{90} = T_{90}/(1+z)$ and $T^*_{45} = T_{45}/(1+z)$.[7] We stress here that $\rho = 0.79$ for the $L_{\rm peak}$–$L_{\rm a}$ correlation, where $L_{\rm peak}$ is computed according to the second BAT catalogue, is considerably increased compared to $\rho = 0.60$ for the $L_{90} = E/T_{90}$ versus $L_{\rm a}$ correlation (Dainotti, Ostrowski & Willingale 2011b). This means that a more suitable choice of the parameters in the luminosities or energies definition can increase of the 24 per cent the correlation coefficient. We also note that here the sample is doubled compared to the analysis performed by Dainotti et al. (2011b) in which the GRBs analysed were 62. In Fig. 6 we selected the value of $L_{\rm peak}$ computed from equation (1) assuming a broken PL or a simple PL as a spectral model (as it has been explained in Section 4) thus not involving error propagation due to time and energy as in the previous defined luminosities. This is the reason why for this correlation we obtain an increment of ρ.

We here underline the importance of the choice of the $L_{\rm peak}$–$L_{\rm a}$ correlation and not of the E–$L_{\rm a}$ correlations presented in Dainotti et al. (2011b), because E may suffer from the systematic bias in duration measurements. This would mean that although E evolution studies may in fact be biased at high redshift where a fraction of detected bursts grow with a low signal-to-noise ratio, no such bias should exist for $L_{\rm peak}$ (Lloyd & Petrosian 1999). Therefore, the luminosity–duration is more reliable than the energy–duration correlation, and in the present paper this is the reason why we addressed the attention to the $L_{\rm peak}$–$L_{\rm a}$ relation, instead of E–$L_{\rm a}$.

6 THE REDSHIFT DEPENDENCE

The $L_{\rm peak}$–$L_{\rm a}$ correlation could be due to the dependence of luminosity on distance, since it involves two luminosities. We compare Figs 6 and 7 in order to clarify how much this dependence influences the existence of the correlation itself. In support of the existence of the $L_{\rm peak}$–$L_{\rm a}$ correlation we show the correlation between observed fluxes $F_{\rm a}$, the flux at time $T_{\rm a}$, versus the peak flux in the prompt emission, $F_{\rm peak}$, $F_{\rm a}$–$F_{\rm peak}$, with a Spearman (1904) correlation coefficient $\rho = 0.63$ (see Fig. 7). Thus, we remove with a first rough approximation the redshift dependence induced by the distance luminosity using fluxes instead of luminosities. In fact, if the $L_{\rm peak}$–$L_{\rm a}$ correlation was completely due to the induced redshift dependence this would have caused a disappearing of the correlation or a drastically reduced value of ρ less than 0.5 and a probability of occurrence by chance >5 per cent, which is not the case. Then, to evaluate

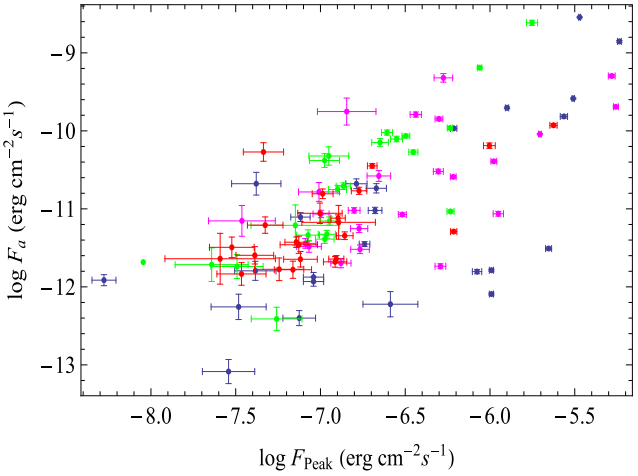

Figure 7. GRB distributions in redshift bins at the $F_{\rm a}$–$F_{\rm peak}$ plane, where $F_{\rm peak}$ is computed following the approach used in the second BAT catalogue. The sample is splited into four different equipopulated redshift bins: $z \leq 0.84$ (blue), $0.84 \leq z < 1.8$ (magenta), $1.8 \leq z < 2.9$ (green) and $z \geq 2.9$ (red). The dashed line is the fitting correlation line.

[7] T^*_{90} and T^*_{45} are the rest-frame time-scales for GRB energy emission between 5 and 95 per cent and 5 and 50 per cent ranges of the total prompt emission, respectively, while T^*_p is the rest-frame time at the end of the prompt emission in the W07 model.

the presence of redshift evolution we follow the approach adopted in Dainotti et al. (2011a, 2013a) by dividing the sample into four redshift bins. The GRBs distribution in each redshift bin is not clustered or confined in a given subspace, see Fig. 6, thus suggesting no strong redshift evolution. This is expected for L_a, because Dainotti et al. (2013a) demonstrated that there is no redshift evolution of this luminosity. However, Petrosian, Kitanidis & Kocevski (2015) show that $L_{\rm peak}$ is affected by the redshift evolution as $L_{\rm peak}/(1+z)^{2.3}$ using a more complex function than the simple PL, used previously for GRBs (Dainotti et al. 2013a). Here the sample has been chosen differently from Petrosian et al. (2015), because only observations which have good coverage of the data in the early prompt and can be fitted within the W010 model are taken into account. Therefore, for a more precise evaluation we have to address the problem of the luminosity evolution for this specific sample. For a quantitative analysis of this problem we apply the Efron & Petrosian (1992) method.

7 THE EFRON AND PETROSIAN METHOD

The first important step for determining the distribution of true correlations among the variables is the quantification of the biases introduced by the observational selection effects due to the selected sample and the instrumental limits. In the case under study the selection effect or bias that distorts the statistical correlations is the flux limit and the temporal resolution of the instrument. To account for these effects we apply the Efron–Petrosian (EP) technique, already successfully applied for GRBs (Lloyd & Petrosian 2000; Kocevski & Liang 2006; Petrosian, Bouvier & Ryde 2009). The EP method reveals the intrinsic correlation because the method is specifically designed to overcome the biases resulting from incomplete data. Moreover, it identifies and removes also the redshift evolution present in both variables, time and luminosity.

The EP method uses a modified version of the Kendall τ statistic to test the independence of variables in a truncated data. Instead of calculating the ranks R_i of each data points among all observed objects, which is normally done for an untruncated data, the rank of each data point is determined among its 'associated sets' which include all objects that could have been observed given the observational limits.

Here we give a brief summary of the algebra involved in the EP method. This method uses the Kendall rank test to determine the best-fitting values of parameters describing the correlation functions using the test statistic,

$$\tau = \frac{\sum_i (\mathcal{R}_i - \mathcal{E}_i)}{\sqrt{\sum_i \mathcal{V}_i}}, \tag{5}$$

to determine the independence of two variables in a data set, say (x_i, y_i) for $i = 1, \ldots, n$. Here R_i is the rank of variable y of the data point i in a set associated with it. For an untruncated data (i.e. data truncated parallel to the axes) the *associated set* of point i includes all of the data with $x_j < x_i$. If the data are truncated one must form the *associated set* consisting only of those points which satisfy conditions imposed by the limiting instrumental values, see definition below.

If (x_i, y_i) were independent then the rank $\mathcal{R}_i$ should be distributed continuously between 0 and 1 with the expectation value $\mathcal{E}_i = (1/2)(i+1)$ and variance $\mathcal{V}_i = (1/12)(i^2-1)$. Independence is rejected at the $n\sigma$ level if $|\tau| > n$. Here the mean and variance are calculated separately for each associated set and summed accordingly to produce a single value for τ. This parameter represents the degree of correlation for the entire sample with proper accounting for the data truncation.

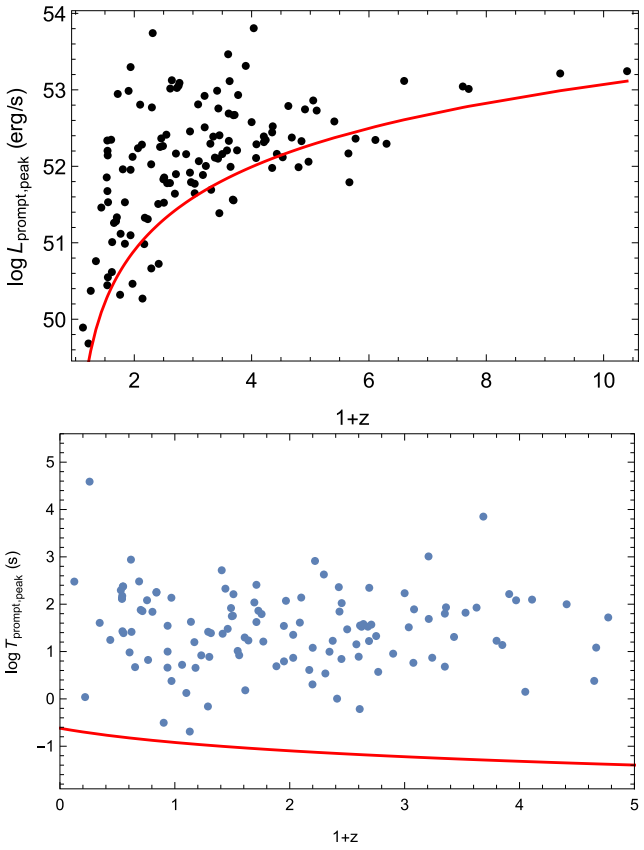

Figure 8. Upper panel: the bivariate distribution of $L_{\rm peak}$ and redshift with the flux limit assuming the K-correction $K = 1$. The BAT flux limit, 4.0×10^{-8} erg cm^{-2} (solid red line) which better represents the limit of the sample. Lower panel: the bivariate distribution of the rest-frame time $T^*_{\rm prompt}$ and the redshift, where with $T_{\rm prompt}$ we denote the sum of the peak pulses width of each single pulse in each GRB. The chosen limiting value of the observed pulse width in the sample, $T_{\rm prompt,\,lim} = 0.24$ s. The red line is the limiting rest-frame time, $T_{\rm prompt,\,lim}/(1+z)$.

With this statistic, we find the parametrization that best describes the luminosity and time evolution for the prompt emission. For the afterglow emission we refer to results already presented in Dainotti et al. (2013a). We now have to determine the limiting flux, $F_{\rm lim}$, which gives the minimum observed luminosity for a given redshift, $L_{\rm lim} = 4\pi D_L^2(z)\, F_{\rm lim} K$. In the upper panel of Fig. 8 we show the limiting luminosity for $K = 1$ just not to show fuzzy boundaries, but for an appropriate evaluation of the luminosity evolution we assign to each GRB its own K-correction. We have investigated several limiting fluxes to determine a good representative value, while keeping an adequate size of the sample itself. We have finally chosen the limiting flux $F_{\rm lim} = 4.0 \times 10^{-8}$ erg cm^{-2}, which allows 116 GRBs in the sample. We have also chosen the observed minimum pulse width of the prompt, which is $T^*_{\rm prompt,lim} = 0.24/(1+z)$ s, lower panel of Fig. 8. This time has been computed as the sum of the single pulses width in each GRB. In such a way we can employ a comparison with previous time evolution in the afterglow as presented in Dainotti et al. (2013a).

7.1 The luminosity and time evolutions

For the luminosity and time evolution it is necessary to first determine whether the variables $L_{\rm peak}$ and $T^*_{\rm prompt}$ are correlated with redshift or are statistically independent. For example, the correlation between $L_{\rm peak}$ and the redshift, z, is what we call luminosity evolution, and independence of these variables would imply absence of such evolution. The EP method prescribed how to remove the correlation by defining new and independent variables.

We determine the correlation functions $g(z)$ and $f(z)$ when determining the evolution of $L_{\rm peak}$ and $T^*_{\rm prompt}$ so that de-evolved variables, namely the local variables, $L'_{\rm peak} \equiv L_{\rm peak}/g(z)$ and $T'_{\rm prompt} \equiv T^*_{\rm prompt}/f(z)$, are not correlated with z. The evolutionary functions are parametrized both by simple correlation functions or more complex ones.

The simple PL functions are represented by

$$g(z) = (1+z)^{k_{L_{\rm peak}}},\ f(z) = (1+z)^{k_{T^*,{\rm prompt}}}, \tag{6}$$

so that $L'_{\rm peak} = L_{\rm peak}/g(z)$ refer to the local ($z = 0$) luminosities. The more complex function chooses a fiducial critical Z, where we define $Z = 1 + z$. We chose $Z_{\rm cr} = 3.5$, thus allowing the following functional form for

$$g(z) = \frac{Z^{k_L}\left(1+Z_{\rm cr}^{k_L}\right)}{Z^{k_L}+Z_{\rm cr}^{k_L}},\ f(z) = \frac{Z^{k^*_T}\left(1+Z_{\rm cr}^{k^*_T}\right)}{Z^{k^*_T}+Z_{\rm cr}^{k^*_T}}. \tag{7}$$

We computed both approaches obtaining compatible results. The associated set for the source i to obtain the luminosity evolution is

$$J_i \equiv \{j : L_j > L_{\rm min}(i)\} \vee \{j : L_j > L_i\} \vee \{j : z_j < z_i\}, \tag{8}$$

where $L_{\rm min}(i)$ is the minimum luminosity of the object i correspondent to L_i, z_i is the redshift of the object i. The objects of all the sample are indicated with i, while the objects in the associated sets are denoted with j. With the symbol $\vee$ we indicate the union of the sets.

Analogously, to obtain the pulse width evolution factor we need to compute the associated set for a given object i, which are

$$J_i \equiv \{j : T_j > T_{{\rm min},i}\} \vee \{j : T_j > T_i\} \vee \{j : z_j > z_i\}, \tag{9}$$

where $T_{\rm min}(T_{{\rm prompt},\,i})$ is the minimum $T_{\rm prompt}$ at which object i could be still included in the survey given its peak width duration and the limiting time of the observation.

With the specialized version of Kendell's τ statistic, the values of $k_{L_{\rm peak}}$ and $k_{T^*_{\rm prompt}}$ for which $\tau_{L_{\rm peak}} = 0$ and $\tau_{T^*{\rm prompt}} = 0$ are the ones that best fit the luminosity and width pulse evolution, respectively, with the 1σ range of uncertainty given by $|\tau_x| \leq 1$. Plots of $\tau_{L_{\rm peak}}$ and $\tau_{T^*_{\rm prompt}}$ versus $k_{L_{\rm peak}}$ and $\tau_{T^*_{\rm prompt}}$ are shown in Figs 9 and 10, respectively. With $k_{L_{\rm peak}}$ and $k_{T^*{\rm prompt}}$ we are able to determine the de-evolved observables $T'_{\rm prompt}$ and $L'_{\rm peak}$.

There is a significant luminosity evolution in the prompt, $k_{L_{\rm peak}} = 2.13^{+0.33}_{-0.37}$, and much less significant in the time, $k_{T^*_{\rm prompt}} = -0.62 \pm 0.38$, for the simple PL functions. If we consider the more complex function for the evolution we obtain $k_{L_{\rm peak}} = 3.09^{+0.40}_{-0.35}$ and $k_{T^*_{\rm prompt}} = -0.17^{+0.24}_{-0.27}$. It is straightforward that we achieve a higher evolution for luminosity and a smaller evolution for the time for the way we chose the function. We also note that the results of the luminosity evolutions among the two different functions are compatible within 2σ, while the time evolutions are compatible within 1σ.

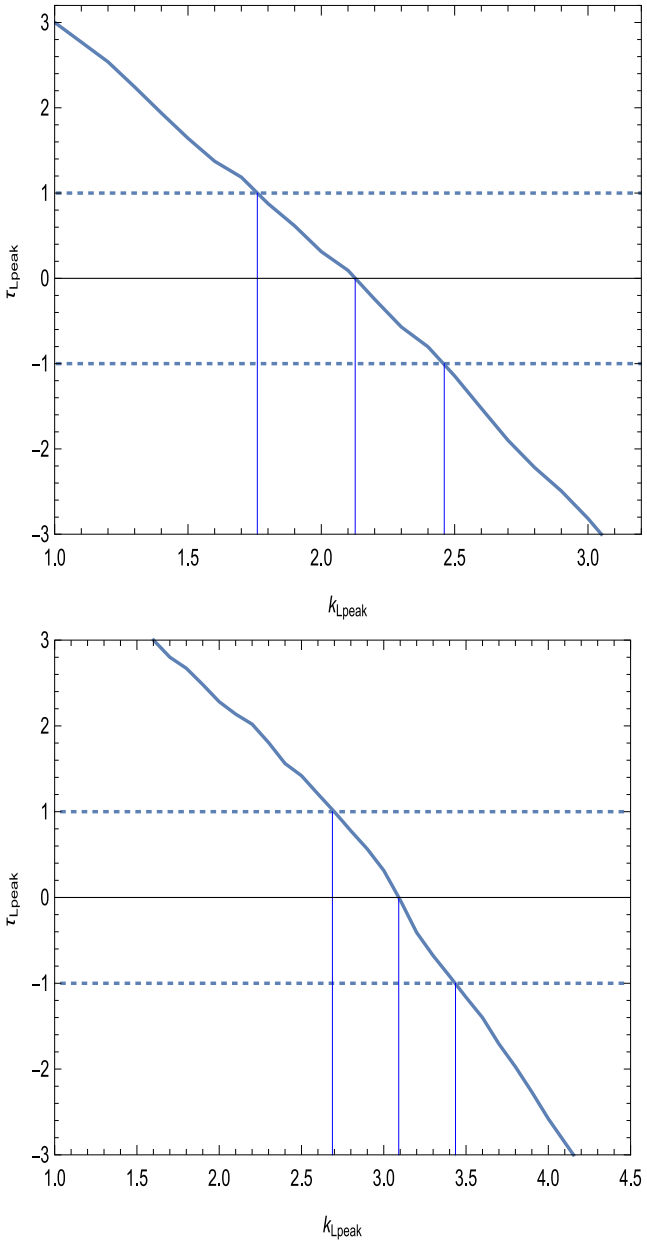

Figure 9. Upper: test statistic τ versus $k_{L_{\rm peak,prompt}}$, the luminosity evolution defined by equation (6) using a simple PL as $g(z)$. Lower: the same test statistic using a more complex function for the evolution $g(z)$, defined by the equation (7).

7.2 The intrinsic $L_{\rm peak}$-$L_{\rm a}$ correlation

We here focus on determining the intrinsic correlation among the local luminosities $L'_{\rm peak}$-$L^*_{\rm a}$.[8] Following the method presented in

[8] Here we do not consider the de-evolved $L'_{\rm peak}$-$T'_{\rm prompt}$ correlation because the $T'_{\rm prompt}$ adopted is the sum of the all time widths of all the pulses for each GRB and not the width of the single pulse. Therefore, we cannot determine with accuracy the evolution in time for the prompt since for single pulses we are not able to apply the EP method, because we have only one limiting time for all the total integrated time over all the pulses and this does not coincide with the minimum time among each single pulse. Thus, this discrepancy in

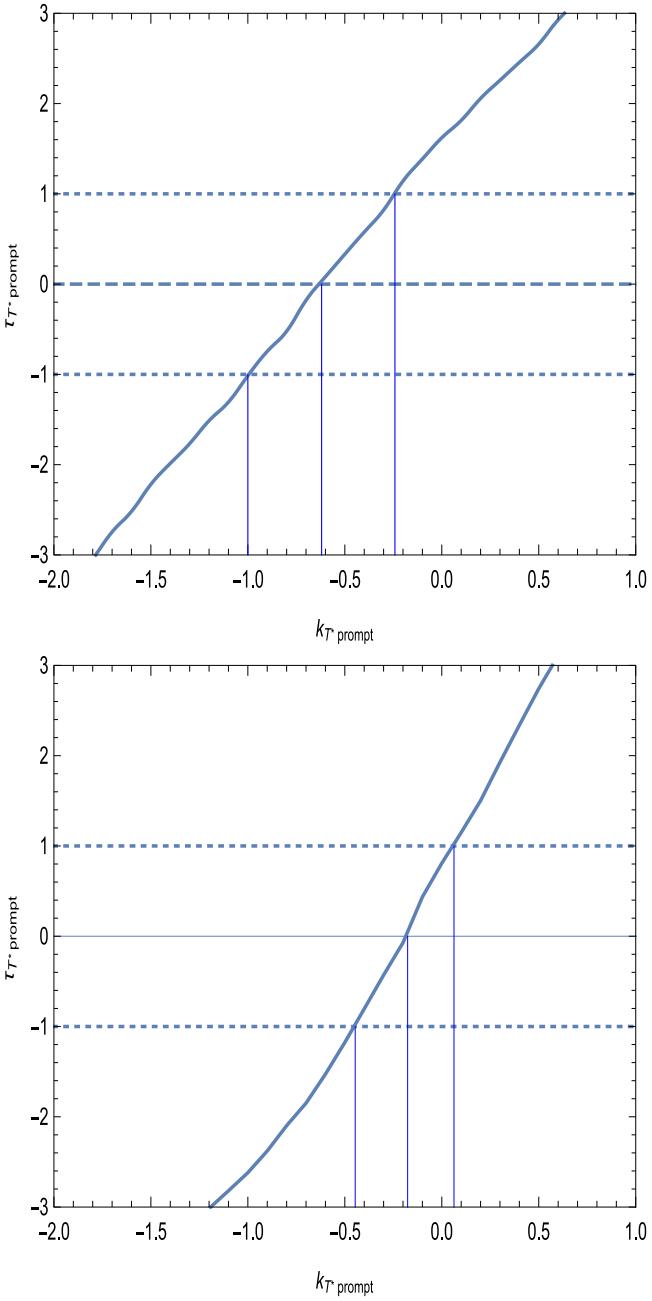

Figure 10. Upper panel: test statistic τ versus $k_{T^*_{\mathrm{prompt}}}$, the time evolution defined by equation (6). Lower panel: the same test statistic using a more complex function for the evolution $g(z)$, defined by the equation (7).

Petrosian & Singal (2014) we compute the dependence of this correlation from the luminosity distance. According to equation (4) we can rename the variables with an abuse of notation for simplicity as $\log L'_{\mathrm{a}} = L'_{\mathrm{a}}$, $\log L'_{\mathrm{peak}} = L'_{\mathrm{peak}}$ and $\log D_L = D_L$ in order to write

the limiting time determination can lead to an inaccuracy in the evaluation of the time evolution. Notwithstanding this difficulty for the time evolution, for the luminosity evolution this problem does not occur, since we chose the maximum peak luminosity of each GRB among the all pulses in that given GRB.

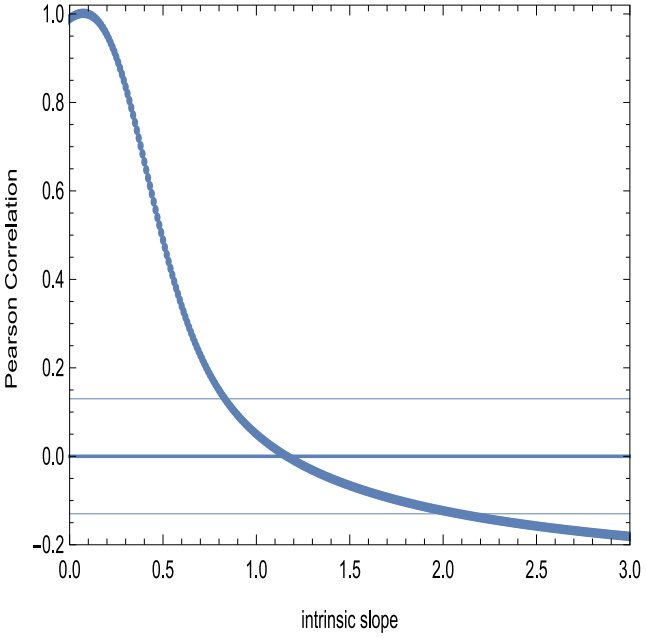

Figure 11. Local luminosity–luminosity correlation coefficient versus the intrinsic slope showing the best value where L'_{peak} and L'_{a} are significantly correlated (the central thick line). The two thinner lines parallel to $r = 0$ show the 0.05 per cent probability that the sample is drawn by chance.

in a simpler way the partial correlation coefficient in the log space domain:

$$r_{L'_{\mathrm{peak}}L'_{\mathrm{a}},D_L} = \frac{r_{L'_{\mathrm{peak}},L'_{\mathrm{a}}} - r_{L'_{\mathrm{peak}},D_L} r_{L'_{\mathrm{a}},D_L}}{\left(1 - r^2_{L'_{\mathrm{peak}},D_L}\right)\left(1 - r^2_{L'_{\mathrm{a}},D_L}\right)}, \tag{10}$$

which accounts for mutual distance dependence of the luminosities. We now consider the correlation in the local luminosity space so that $L''_{\mathrm{a}} = L'_{\mathrm{peak}} - \alpha L'_{\mathrm{a}}$ and we calculate the $r_{L'_{\mathrm{peak}},L'_{\mathrm{a}},D_L}$ as a function of the index α, namely the intrinsic slope. As shown in Fig. 11 the correlation becomes significant for $\alpha = 1.14^{0.83}_{-0.32}$, which is very close to the observed correlation. The error bars quoted are at the 2σ significance level.

8 SUMMARY AND DISCUSSION

The analysis presented in this study reveals that the following.

(i) Prompt and plateau phases dissipate similar amounts of energy, but over very different time scales as shown through Figs 1, 2 and 5.

(ii) Slopes in the luminosity–duration distributions between the prompt and plateau emissions L_{f}-T^*_{f} versus L_{a}-T^*_{a} differ almost 3σ, while in the local luminosity space more than 3σ. However, for the evaluation of the time evolutions of the pulse in the prompt there is the problem of determining the proper limiting time of the pulses, as we explained in Footnote 8. Therefore, a definite conclusion on the differences in the slopes still needs to be reached and this will be object of a forthcoming investigation. The evidence of difference between prompt and afterglow is then recalled also by the difference in the spectral parameters of the prompt and the afterglow phases. Also this fact does not imply necessarily a diverse mechanism as we have pointed out in Section 5.2.

(iii) The extended luminosity–duration distributions L_{f}-T^*_{f}, see upper panel of Fig. 2, and the energy–duration correlation, see the middle panel of Fig. 2, show that there is continuity in

transition from prompt distribution to the afterglow one, namely no gap in the data. Difference between the prompt and plateau slopes is present independently from the choice of luminosity or energy. The luminosity–duration and energy–duration spaces are just two ways of looking at the same data, as well as the difference in the correlations. The $E_{\rm total}$–duration plot in the lower panel of Fig. 2 clearly shows that the plateaus occupy a different area of the energy–duration plane to the pulses. Individual prompt pulses and plateaus both produce energy values in the same broad range, but the plateau duration is on average a factor of 100 larger.

(iv) Stronger correlations are present when we compare, respectively, $\langle L_{\rm prompt}\rangle - L_{\rm a}$ and $L_{\rm peak}$–$L_{\rm a}$ luminosities, see Fig. 6, rather than considering $L_{\rm a}$ and the prompt emission luminosities computed as ratio of energy over a particular time-scale, such as $L_{45} = E/T_{45}$ and $L_{90} = E/T_{90}$, (Dainotti et al. 2011b).

(v) We found very interestingly that the $L_{\rm peak}$–$L_{\rm a}$ correlation is very robust also in the local luminosity space when we removed the luminosity evolution both in the prompt and in the afterglow and it presents a compatible result of the intrinsic slope with the observed slope within 1σ. This will have impact on the investigation for the theoretical models.

From this analysis we hypothesize that the following.

(i) Both the different slopes in the luminosity–duration and in the energy–duration space of prompt pulses and plateau ones might indicate that these two are quite distinct features of the emission. The former probably come from internal shocks and the latter from the external shock. The prompt pulses are fast cooling while the plateau pulses are slow cooling. This is known from the literature for the prompt and afterglow phases (Rees & Meszaros 1994, 1998), but the upper panel of Fig. 2 shows that this statement might be true also for the plateau phase. So this is another significant difference between the prompt and plateau phase indicating that if the latter is due to synchrotron from the external shock (which is likely), then the pulses all have very similar physical conditions in the shock. In particular, the PL index of the electron distribution is very similar in all cases.

(ii) The present study is relevant to quantify the mentioned relations in order to improve or modify the existing physical model of GRB emission which should predict the $L_{\rm peak}$ versus $L_{\rm a}$ correlation together with the combined L–T correlations both in prompt and afterglow phases. In particular, among the models we have mentioned in the theoretical motivation of this work the one that better describe the observed correlations is the model by Hascoet et al. (2014), because some particular configurations of the microphysical parameters are able to reproduce the L–T correlations difference in slopes and the $\langle L_{\rm prompt}\rangle$–$L_{\rm a}$ correlations. Also the model proposed by Ruffini et al. (2014) is able to reproduce these observational features, while thin shell models, (Van Erten 2014b), are ruled out.

In conclusion, all these observational evidences taken into account contemporaneously are able to better test and discriminate some of the existing theoretical models.

ACKNOWLEDGEMENTS

This work made use of data supplied by the UK Swift Science Data Centre at the University of Leicester. We are grateful to M. Barkov and F. Rubio Da Costa for useful comments and remarks on the manuscript. MD is grateful for the initial support from the JSPS (No. 25.03786). Moreover, the research leading to these results has received funding from the European Union Seventh Framework Programme (FP7/2007-2013) under grant agreement no. 626267. MD and SN are grateful to the iTHES Group discussions at Riken. MD is also grateful to RW and PO'B to be hosted by the Astronomy Department at Leicester University through their department grant. MO is grateful to the Polish National Science Centre for support through the grant DEC-2012/04/A/ST9/00083. SN is grateful to JSPS (No. 24.02022, No. 25.03018, No. 25610056, No. 26287056) and MEXT(No. 26105521).

REFERENCES

Amati L. et al., 2002, A&A, 390, 81
Amati L., Frontera F., Guidorzi C., 2009, A&A, 508, 173
Band D. et al., 1993, ApJ, 413, 281
Barkov M., Pozanenko A., 2011, MNRAS, 417, 2161
Bernardini M. G., Margutti R., Zaninoni E., Chincarini G., 2012a, MNRAS, 425, 1199
Bernardini M. G., Margutti R., Mao J., Zaninoni E., Chincarini G., 2012b, A&A, 539, A3
Bevington P. R., Robinson D. K., 2003, Data Reduction and Error Analysis for the Physical Sciences, 3rd edn. McGraw-Hill, New York
Bloom J. S., Frail D. A., Sari R., 2001, AJ, 121, 2879
Butler N. R., Kocevski D., Bloom J. S., Curtis J. L., 2007, ApJ, 671, 656
Butler N. R., Kocevski D., Bloom J. S., 2009, ApJ, 694, 76
Cabrera J. I., Firmani C., Avila-Reese V., Ghirlanda G., Ghisellini G., Nava L., 2007, MNRAS, 382, 342
Cannizzo J. K., Gehrels N., 2009, ApJ, 700, 1047
Cannizzo J. K., Troja E., Gehrels N., 2011, ApJ, 734, 35
Cardone V. F., Capozziello S., Dainotti M. G., 2009, MNRAS, 400, 775
Cardone V. F., Dainotti M. G., Capozziello S., Willingale R., 2010, MNRAS, 408, 1181
Collazzi A. C., Schaefer B. E., 2008, ApJ, 688, 456
D'Agostini G., 2005, preprint (arXiv:physics/0511182)
Dainotti M. G., Bernardini M. G., Bianco C. L., Caito L., Guida R., Ruffini R., 2007, A&A, 471, L29
Dainotti M. G., Cardone V. F., Capozziello S., 2008, MNRAS, 391, L79
Dainotti M. G., Willingale R., Capozziello S., Cardone V. F., Ostrowski M., 2010, ApJ, 722, L215
Dainotti M. G., Cardone V. F., Capozziello S., Ostrowski M., Willingale R., 2011a, ApJ, 730, 135
Dainotti M. G., Ostrowski M., Willingale R., 2011b, MNRAS, 418, 2202
Dainotti M. G., Petrosian V., Singal J., Ostrowski, 2013a, ApJ, 774, 157
Dainotti M. G., Cardone V. F., Piedipalumbo E., Capozziello S., 2013b, MNRAS, 436, 82
Dainotti M. G., Del Vecchio R., Nagataki S., Capozziello S., 2015, ApJ, 800, 31
Dall'Osso S., Stratta G., Guetta D., Covino S., De Cesare G., Stella L., 2011, A&A, 526, A121
Dermer C., 2007, ApJ, 664, 384
Efron B., Petrosian V., 1992, ApJ, 399, 345
Evans P. A. et al., 2009, MNRAS, 397, 1177
Evans P. A. et al., 2010, A&A, 519, A102
Evans P. A. et al., 2014, MNRAS, 444, 250
Fenimore E. E., Ramirez-Ruiz E., 2000, ApJ, 539, 712
Ghirlanda G., Ghisellini G., Lazzati D., 2004, ApJ, 616, 331
Ghirlanda G., Ghisellini G., Firmani C., 2006, New J. Phys., 8, 123
Ghisellini G., Nardini M., Ghirlanda G., Celotti A., 2009, MNRAS, 393, 253
Guida R., Bernardini M. G., Bianco C. L., Caito L., Dainotti M. G., Ruffini R., 2008, A&A, 487, L37
Hascoët R., Daigne F., Mochkovitch R., 2014, MNRAS, 442, 20
Ito H., Nagataki S., Matsumoto J., Lee S.-H., Tolstov A., Mao J., Dainotti M., Mizuta A., 2014, ApJ, 789, 159
Izzo L., Pisani G. B., Muccino M., Rueda J. A., Wang Y., Bianco C. L., Penacchioni A. V., Ruffini R., 2012, in Castro-Tirado A. J., Gorosabel

J., Park I. H., eds, EAS Publ. Ser. Vol. 61, Gamma-Ray Bursts: 15 Years of GRB Afterglows. EDP Sciences, France, p. 595
Kocevski D., Liang E., 2006, ApJ, 642, 371
Leventis K., Wijers R. A. M. J., van der Horst A. J., 2014, MNRAS, 437, 2448
Lloyd N., Petrosian V., 1999, ApJ, 511, 550
Lloyd N., Petrosian V., 2000, ApJ, 543, 722
Margutti R. et al., 2013, MNRAS, 428, 729
Nemmen R. S., Georganopoulos M., Guiriec S., Meyer E. T., Gehrels N., Sambruna R. M., 2012, Science, 338, 1445
O'Brien P. T. et al., 2006, ApJ, 647, 1213
O'Brien P. T., Lyons N., Rowlinson A., 2011, AIP Conf. Proc., Vol. 1358, Gamma Ray Bursts. 2010. Am. Inst. Phys., New York, p. 319
Petrosian V., Singal J., 2015, in Massaro F., Cheung C. C., Lopez E., Siemiginowska A., eds, Proc. IAU Symp. 313, Extragalactic Jets from Every Angle. Cambridge Univ. Press, Cambridge, p. 333
Petrosian V., Bouvier A., Ryde F., 2009, preprint (arXiv:0909.5051)
Petrosian V., Kitanidis E., Kocevski D., 2015, ApJ, 806, 44
Postnikov S., Dainotti M. G., Hernandez X., Capozziello S., 2014, ApJ, 783, 126
Qi S., Lu T., 2010, ApJ, 717, 1274
Rees M. J., Meszaros P., 1994, ApJ, 430, L93
Rees M. J., Meszaros P., 1998, ApJ, 496, L1
Riechart D. E., Lamb D. Q., Fenimore E. E., Ramirez-Ruiz E., Cline T. L., 2001, ApJ, 552, 57
Rowlinson A., O'Brien P. T., Metzger B. D., Tanvir N. R., Levan A. J., 2013, MNRAS, 430, 1061
Rowlinsown A., Gompertz B. P., Dainotti M., O'Brien P. T., Wijers R. A. M. J., van der Horst A. J., 2014, MNRAS, 443, 1779
Ruffini R. et al., 2014, A&A, 565L, 10
Ryde F., Petrosian V., 2002, ApJ, 578, 290
Sakamoto T. et al., 2007, ApJ, 669, 1115
Sakamoto T. et al., 2011, ApJS, 195, 2
Schaefer B. E., 2003, ApJ, 583, L67
Schaefer B., 2007, ApJ, 660, 16
Shahmoradi A., Nemiroff R., 2009, in Meegan C., Kouveliotou C., Gehrels N., eds, AIP Conf. Proc. Vol. 1133, Gamma-Ray Burst: Sixth Huntsville Symposium. Am. Inst. Phys., New York, p. 425
Spearman C., 1904, Am. J. Psychol., 15, 72
Sultana J., Kazanas D., Fukumura K., 2012, ApJ, 758, 32
Sultana J., Kazanas D., Mastichiadis A., 2013, ApJ, 779, 16
Van Erten H., 2014a, MNRAS, 442, 3495
Van Erten H., 2014b, MNRAS, 445, 2414
Willingale R. W. et al., 2007, ApJ, 662, 1093 (W07)
Willingale R., Genet F., Granot J., O'Brien P. T., 2010, MNRAS, 403, 1296 (W10)
Xiao L., Schaefer B. E., 2009, ApJ, 707, 387
Yamazaki R., 2009, ApJ, 690, L118
Yonetoku D., Murakami T., Nakamura T., Yamazaki R., Inoue A. K., Ioka K., 2004, ApJ, 609, 935
Yu B., Qi S., Lu T., 2009, ApJ, 705, L15

APPENDIX A: THE D'AGOSTINI FITTING METHOD

We briefly present the D'Agostini method (D'Agostini 2005), used to fit the above mentioned correlations. This takes into account the intrinsic scatter, thus providing more reliable errors. Let us suppose that R and Q are two quantities related by a linear relation

$$R = aQ + b, \tag{A1}$$

and denote with $\sigma_{\rm int}$ the intrinsic scatter around this relation. Calibrating such a relation means determining the two coefficients (a, b) and the intrinsic scatter $\sigma_{\rm int}$. To this aim, we will resort to a Bayesian motivated technique (D'Agostini 2005) thus maximizing the likelihood function $\mathcal{L}(a, b, \sigma_{\rm int}) = \exp[-L(a, b, \sigma_{\rm int})]$ with

$$L(a, b, \sigma_{\rm int}) = \frac{1}{2}\sum \ln L_1 + \frac{1}{2}\sum \ln L_2, \tag{A2}$$

where

$$L_1 = (\sigma_{\rm int}^2 + \sigma_{R_i}^2 + a^2\sigma_{Q_i}^2) \tag{A3}$$

and

$$L_2 = \frac{(R_i - aQ_i - b)^2}{\sigma_{\rm int}^2 + \sigma_{Q_i}^2 + a^2\sigma_{Q_i}^2}, \tag{A4}$$

where the sum is over the $\mathcal{N}$ objects in the sample. The above formulae easily applies to our case setting $R = \log L_{\rm X}^*(T_{\rm a})$ and $Q = \log T_{\rm a}^*$. We estimate the uncertainty on $\log L_{\rm X}^*(T_{\rm a})$ by propagating the errors on $(T_{\rm a}, F_{\rm a}, \beta_{\rm a})$.

The Bayesian approach used here also allows us to quantify the uncertainties on the fit parameters. To this aim, for a given parameter p_i, we first compute the marginalized likelihood $\mathcal{L}_i(p_i)$ by integrating over the other parameter. The median value for the parameter p_i is then found by solving

$$\int_{p_{i,\rm min}}^{p_{i,\rm med}} \mathcal{L}_i(p_i)\mathrm{d}p_i = \frac{1}{2}\int_{p_{i,\rm min}}^{p_{i,\rm max}} \mathcal{L}_i(p_i)\mathrm{d}p_i. \tag{A5}$$

The 68 per cent (95 per cent) confidence range $(p_{i,\,l},\, p_{i,\,h})$ are then found by solving

$$\int_{p_{i,\rm l}}^{p_{i,\rm med}} \mathcal{L}_i(p_i)\mathrm{d}p_i = \frac{1-\varepsilon}{2}\int_{p_{i,\rm min}}^{p_{i,\rm max}} \mathcal{L}_i(p_i)\mathrm{d}p_i, \tag{A6}$$

$$\int_{p_{i,\rm med}}^{p_{i,\rm h}} \mathcal{L}_i(p_i)\mathrm{d}p_i = \frac{1-\varepsilon}{2}\int_{p_{i,\rm min}}^{p_{i,\rm max}} \mathcal{L}_i(p_i)\mathrm{d}p_i, \tag{A7}$$

with $\varepsilon = 0.68$ (0.95) for the 68 per cent (95 per cent) range, respectively.

The a and b parameters are independent and the computation of the error is performed around the actual variable and not in the barycentre of points.

This paper has been typeset from a TEX/LATEX file prepared by the author.